OH Radical Initiated Oxidation of 1,3-Butadiene: Isomeric Selective Study of the Dominant Addition Channel

Buddhadeb Ghosh, Alejandro Bugarin, Brian T. Connell, and Simon W. North*

Department of Chemistry, Texas A&M University, P.O. Box 30012, College Station, Texas 77842

Received: January 24, 2010; Revised Manuscript Received: March 17, 2010

We report the first isomeric selective kinetic study of the dominant isomeric pathway in the OH initiated oxidation of 1,3-butadiene in the presence of O_2 and NO using the laser photolysis−laser induced fluorescence (LP-LIF) technique. The photodissociation of the precursor 2-iodo-but-3-en-1-ol results exclusively in the dominant OH−butadiene addition product, permitting important insight into the OH initiated oxidation mechanism. On the basis of analysis of the time dependent OH/OD signals, we have determined a rate constant for O_2 addition to the hydroxyalkyl radical of $7.0^{+7.0}_{-3.0} \times 10^{-13}$ cm^3 s^{-1}, and we find a value of $1.5^{+1.0}_{-0.6} \times 10^{-11}$ cm^3 s^{-1} for the overall reaction rate constant of the hydroxy peroxy radical with NO. We also report the first clear experimental evidence of the (*E*) form of the δ-hydroxyalkoxy channel through isotopic labeling experiments and provide an upper bound of $13 \pm 5\%$ to its branching ratio. This species provides a mechanistic pathway for the formation of 4-hydroxy-2-butenal, which has been identified as a first generation end product. This isomeric selective kinetic study, together with a previous study on the minor channel of the 1,3-butadiene oxidation, yields a comprehensive picture of butadiene oxidation under high NOx conditions relevant to most regions in the continental US.

I. Introduction

1,3-Butadiene is an anthropogenic hydrocarbon, emitted into the atmosphere primarily as a combustion byproduct with automobile exhaust contributing ~80% to the total 1,3-butadiene emission in U.S.A.[1] Other sources of 1,3-butadiene include open burning (~15% contribution) and industrial emissions resulting in atmospheric concentrations ranging from 0.1 to 15.0 ppb.[1–3] 1,3-Butadiene is one of the most important bulk chemicals with an annual production rate of 6 million tons.[4] It is also a significant toxic pollutant,[1] recognized as a known human carcinogen[5,6] with a 30 times higher unit risk factor than that of benzene[3] and a known mutagen.[7] In the troposphere, removal of 1,3-butadiene is initiated by its reaction with OH, Cl, NO_3, and O_3 although the dominant removal process is the reaction with OH.[8–11] Developing a detailed tropospheric oxidation mechanism for 1,3-butadiene is vital for improving air quality model for toxic chemicals which guide regulatory policies.

The addition of OH to either the terminal or the inner carbons in 1,3-butadiene results in two distinct hydroxy alkyl isomers (Figure 1) with an overall rate constant of $(7.0 \pm 0.5) \times 10^{-11}$ molecule^{-1} cm^3 s^{-1}.[9] On the basis of their study of the peroxy radical kinetics resulting from OH initiated 1,3-butadiene oxidation, Jenkin et al. recommended a branching ratio between isomers I and II of 0.87 to 0.13.[12] The subsequent chemistry of each hydroxy alkyl isomer is distinct and leads to unique first generation end products. The differences in the chemistries of isomers I and II originate from their reaction with molecular oxygen. The hydroxyalkyl radical generated by OH addition to a terminal carbon (isomer I) reacts with oxygen to form a peroxy radical.[12] Under high NOx conditions, the peroxy radical formed from isomer I reacts with NO to form an alkoxy radical, with a minor channel leading to the formation of organic nitrate.[8] The alkoxy radicals ultimately form carbonyl/hydroxy carbonyl compounds as the first generation end products, as observed in end product analysis studies.[8] In contrast, the minor hydroxy alkyl radical (isomer II) isomerizes to an α-hydroxyalkyl radical via a cyclic intermediate and subsequently reacts with oxygen via H abstraction to form a C4 carbonyl compound.[13]

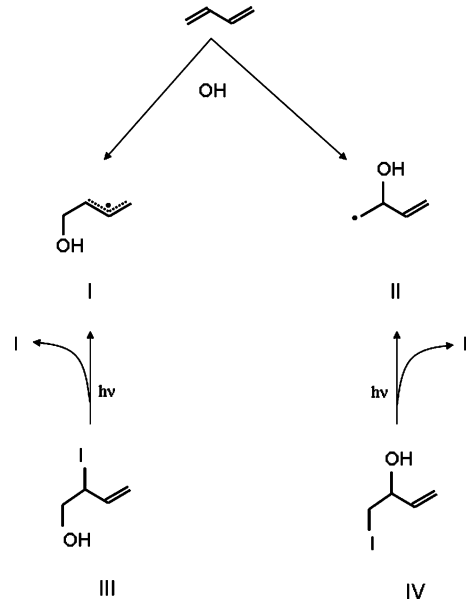

Figure 1. Initial branching of hydroxy alkyl radicals following reaction of OH radical with 1,3-butadiene.

In spite of the importance of 1,3-butadiene oxidation in atmospheric chemistry modeling, there have been few detailed studies of the oxidation mechanism. In the case of isoprene, theoretical studies have demonstrated that the β-hydroxy alkoxy radicals undergo decomposition to form carbonyl compounds and HCHO.[14–16] The δ-hydroxy alkyl isomers, however, undergo a prompt 1,5 H shift followed by H abstraction by oxygen to

* Corresponding Author.

10.1021/jp1006878
Published on Web 04/02/2010

form hydroxy carbonyl compounds.[17–19] Since isoprene is structurally similar to 1,3-butadiene, it is reasonable to assume that 1,3-butadiene will exhibit similar chemistry and that the associated β-hydroxy alkoxy radicals lead to the formation of acrolein. Unlike isoprene, in 1,3-butadiene oxidation only the *Z*-form of hydroxy alkoxy radicals undergoes a 1,5 H shift, leading to the formation of 4-hydroxy-2-butenal. Although the *E*-isomer does not undergo a 1,5 H shift due to the absence of the methyl group, it still leads to the formation of 4-hydroxy-2-butenal. Hydrogen abstraction by O_2 during the oxidation process results in HO_2 radicals which, under high NO conditions, react with NO to regenerate OH radicals. Thus, the time-dependent kinetics of OH in the presence of known concentrations of NO and O_2 can be a sensitive probe of the detailed mechanism of the oxidation process.

In our recent study of the OH initiated oxidation of isoprene, we demonstrated that isomeric selective studies can provide considerable mechanistic insight.[20,21] Photodissociation of suitable precursors enables routes to the formation of energy selected single isomers, enabling the study of important channels that are often difficult to unravel in non-isomer specific experiments. Previously, Greenwald et al. have reported isomeric selective studies of isomer II in 1,3-butadiene oxidation.[13] Here, we focus on the major channel of the 1,3-butadiene oxidation using the photolysis of the precursor 1-hydroxy-2-iodo-3-butene. In doing so, we reduce the complex chemistry of 1,3-butadiene oxidation to a single isomeric pathway permitting determination of isomeric selective rate constants and insight into the mechanism.

Although end product studies have observed acrolein[8,22] and 4-hydroxy-2-butenal,[4] the associated isomeric specific rate constants of different reactions and the branching between the β- and the δ-hydroxy alkoxy radicals have only been inferred. The *E*- and *Z*-isomers of the δ-hydroxy alkoxy radical both lead to the identical first generation end products, but there has been no direct measurement of the branching between these isomers due to the complex nature of chemistry. We find that isotopically labeled cycling experiments can be used to estimate the branching ratio of the *E*-channel.

II. Experimental Section

The precursor compound 1-hydroxy-2-iodo-3-butene was synthesized by adding 57% hydroiodic acid to a mixture of 1 mL of butadiene monoxide in 20 mL of H_2O (kept in dark at 0 C) slowly over a 5 min period. The resulting mixture was stirred for an additional 5 min at 0 C. The reaction mixture was quenched with saturated $Na_2S_2O_7$ solution, and the aqueous layer was extracted with ethyl acetate and then dried with Na_2SO_4. The sample was concentrated under reduced pressure to give the desired pure primary alcohol as colorless oil. The product was identified by NMR, mass spectrometry, and IR spectroscopy (provided in the Supporting Information).

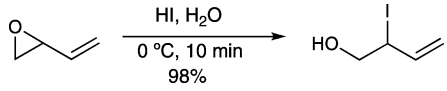

A detailed description of the laser photolysis−laser induced fluorescence (LP/LIF) experiment has been given elsewhere,[23,24] and only the salient features are presented here. A 248 nm photolysis beam from an XE10 excimer laser (GAM Laser) was aligned collinearly through the LIF cell with a probe beam at 282 or 287 nm used for LIF detection of OH or OD, respectively. The probe beam was generated by doubling the output of a dye laser (Quantel TDL-51) running Rhodamine 590 dye or a mixture of Rhodamine 590 and Rhodamine 610 dye pumped by a 532 nm beam from the second harmonic of an Nd YAG laser (Spectra-Physics INDI). The OH/OD fluorescence was monitored by exciting OH/OD at the Q_1 (1) transition of the A ← X (1, 0). A set of lenses was used to collect the fluorescence, and the filtered signal was detected by a photomultiplier tube (PMT) and integrated using a digital oscilloscope. A digital delay generator (SRS, DG-535) was used to control the delay between the two lasers. The precursor was introduced inside the reaction cell through an MKS flow meter by flowing argon through a bubbler containing room temperature sample (vapor pressure ~1.5 Torr). NO (Sigma Aldrich, 98.5%) was purified to remove HONO and NO_2 by using an ascarite trap before buffering with argon in a 5 L tank and introduction into the chamber through an MKS flow meter. The NO concentration was varied from 3.2×10^{14} to 1.9×10^{15} molecules cm^{-3} and the O_2 concentration was varied from 6.5×10^{15} to 6.5×10^{16} molecules cm^{-3}. The temperature of the reaction cell was maintained at room temperature (298 ± 3 K), and an MKS baratron was used to monitor the total pressure inside the cell which was buffered to 50 ± 1 Torr with argon.

TABLE 1: A summary of the experimental conditions employed in the present study

[Precursor] (10^{13} molecules/cm^3)	[NO] (10^{14} molecules/cm^3)	[O_2] (10^{15} molecules/cm^3)
	OH Cycling Experiments from IC_4H_6OH	
3.0	5.0	6.5
3.0	5.0	13.1
3.0	3.2	49.1
3.0	3.2	65.5
3.0	6.4	65.5
3.0	9.6	65.5
3.0	12.8	65.5
3.0	17.0	65.5
3.0	19.0	65.5
	OD Cycling Experiments from IC_4H_6OD	
1.5	11.5	32.8
1.4	13.9	32.8
4.0	19.3	32.8

III. Results and Discussion

We first discuss the results obtained from OH cycling experiments involving the nondeuterated precursor molecule and the corresponding modeling of data including sensitivity analysis of the rate constants. Next we present OD cycling experiments using a deuterated precursor molecule and determination of the branching of the *E*-δ-hydroxy peroxy radical channel.

A. OH Cyling from a Nondeuterated Precursor. In these experiments, the nondeuterated precursor molecule was photolyzed by the 248 nm laser pulse to generate the hydroxy alkyl radical I (Figure 1), which, in the presence of O_2 and NO, produces OH radical, monitored by LIF, through a series of reactions. All experiments were performed under moderate to high NO concentration conditions to ensure rapid OH cycling. In addition, oxygen concentrations higher than the NO concentrations were employed to guarantee higher production rates for OH than loss rates due to radical termination. A summary of the species concentrations for these experiments is tabulated in Table 1. A simplified mechanism for OH cycling is shown in Figure 2.

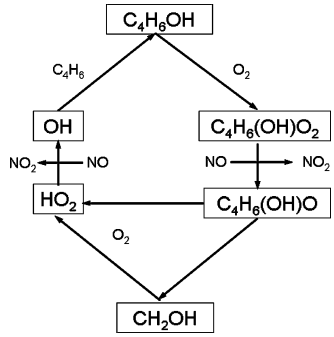

Figure 2. Schematic diagram of OH cycling in 1,3-butadiene oxidation.

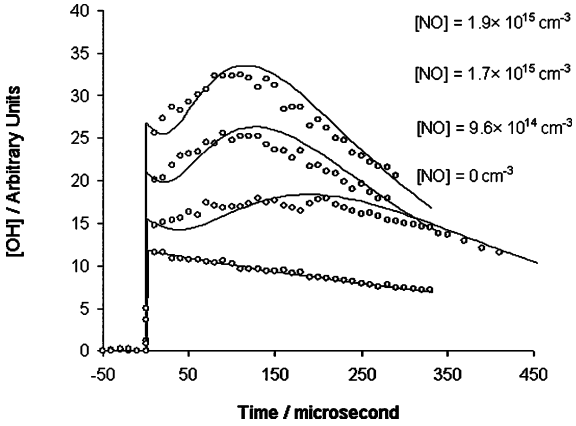

Figure 3. OH fluorescence intensity plotted against reaction time at multiple NO concentrations. Symbols represent experimental data and solid lines represent the fits using the reaction mechanism and rate constants in Table 2. The individual plots have been shifted vertically for clarity. $[IC_4H_6OH] = 3.0 \times 10^{13}$ molecules cm^{-3}, $[O_2] = 6.5 \times 10^{16}$ molecules cm^{-3}. The lowest plot was taken in the absence of NO.

Figure 3 shows a representative data set obtained from OH cycling experiments where the concentration of the precursor molecule was 3.0×10^{13} molecules cm^{-3}, $[O_2] = 6.5 \times 10^{16}$ molecules cm^{-3}, and [NO] was varied from 9.6×10^{14} molecules cm^{-3} to 1.9×10^{15} molecules cm^{-3}. The circles represent the data points, and the solid lines represent the best fit simulation to the data using the mechanism described in Figure 4 and tabulated data in Table 2. The prompt rise in the signal following the photolysis laser pulse is due to the fraction (25%) of the nascent hydroxy alkyl radicals formed with energy exceeding the OH + 1,3-butadiene reaction threshold. In the absence of NO or O_2, the signal decays exponentially as the prompt OH radicals react with the precursor molecule with a rate constant of $k_{20} = 3.0 \times 10^{-11}$ cm^3 s^{-1}. Similar values for this rate constant were observed for analogous iodohydrins.[3,21] In the presence of O_2 and NO, the hydroxy alkyl radical undergoes a series of reactions to form OH. Under these conditions, the OH signal increases to maxima at times ranging from 100 to 200 μs and decreases at long times.

The analysis program KINTECUS[25] was used to simulate the time dependent OH concentrations and perform the associated sensitivity analysis. A set of 22 reactions was used to simulate the data and is provided in Table 2. A more detailed oxidation mechanism for isomer I is shown schematically in Figure 4.

One objective of the study was determination of rate constants for intermediate reaction steps by modeling the OH cycling data. The comprehensive mechanism employed in the fitting procedure includes all the intermediate reactions. Despite the large

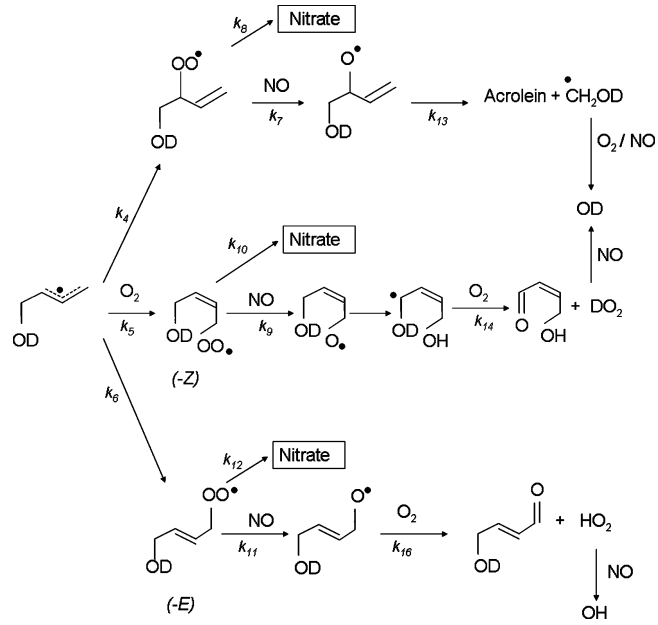

Figure 4. Oxidation mechanism of isomer I.

number of reactions, the simulations are sensitive to a limited number of the rate constants and several of the rate constants are well-known.[26] To assess which reactions have significant effect on the simulations and to guide the choice of experimental conditions, we have used sensitivity analysis.[27] The normalized sensitivity coefficients (NSC) describe the fractional change of the simulations, in this case the OH concentration, at a specific reaction time given a fractional change of each rate constant keeping all other rate constants fixed.

Figure 5 shows the sensitivity analysis calculated at a reaction time of 80 μs, an O_2 concentration of 6.5×10^{16} cm^{-3}, and two different NO concentrations of 9.6×10^{14} cm^{-3} and $[NO] = 1.9 \times 10^{15}$ cm^{-3}. It is clear from the plots that the OH simulations depend sensitively only on few rate constants, specifically the initial branching between the dissociating hydroxyl alkyl radical and the collisionally stabilized hydroxyl alkyl radical (k_1 and k_2), the NO addition to the hydroxyl alkyl radical (k_3), the O_2 addition to the same (k_4), the NO reaction to the hydroxyl peroxy radical (k_7), and the reaction of NO and HO_2 radical (k_{21}). Of these rate constants, the NO reaction rate with HO_2 has been well studied, and we have used the recommended literature value.[28] The absolute values of k_1 and k_2 are unimportant since both are instantaneous on the time scale of the experiments, and only their *relative* magnitudes are important. We have assumed a value of 75% for the thermalized hydroxyl alkyl radicals, which is close to the value used in the study of the dominant channel of OH−isoprene oxidation.[21] The remaining three rate constants with high NSC (k_3, k_4, and k_7) are the focus of the analysis, and we seek to extract their values.

The termination reactions by NO with alkyl and alkoxy radicals (k_{15} and k_{17} respectively) are important at the moderate to high NO concentrations employed in the study to ensure fast cycling. However, the cycling experiments are not particularly sensitive to the precise values of these rate constants, as evident from the sensitivity analysis, and we have used a value of 3.0×10^{-11} cm^3 s^{-1} based on our previous cycling study.[27] We note that this value is close to the other values reported for similar systems.[29–31] The NO addition to hydroxyl 1,3-butadiene (k_3), however, has an appreciable NSC, and we have determined a best fit value of 2.0×10^{-11} cm^3 s^{-1} for this reaction. This value is very similar to the value of 2.2×10^{-11} cm^3 s^{-1} reported

TABLE 2: Reaction Mechanism and Corresponding Rate Constants (298 K) Used for Simulation of the Experimental Data[a]

	reaction		rate constant	ref	comment
k_1	$HOC_4H_6 \rightarrow$	$OH + C_4H_6$	prompt (25%)	*b*	"prompt" OH
k_2	$HOC_4H_6 \rightarrow$	HOC_4H_6	prompt (75%)	*b*	OH cycling
k_3	$HOC_4H_6 + NO \rightarrow$	HOC_4H_6NO	2.0×10^{-11}	*b*	
k_4	$HOC_4H_6 + O_2 \rightarrow$	β-$HOCH_2CH(O_2)CH{=}CH_2$	5.25×10^{-13}	*b*	β-branching
k_5	$HOC_4H_6 + O_2 \rightarrow$	*Z*-$HOCH_2CH{=}CHCH_2O_2$	8.75×10^{-14}	*b*	*Z*-δ-branching
k_6	$HOC_4H_6 + O_2 \rightarrow$	*E*-$HOCH_2CH{=}CHCH_2O_2$	8.75×10^{-14}	*b*	*E*-δ-branching
k_7	β-$HOCH_2CH(O_2)CH{=}CH_2 + NO \rightarrow$	β-$HOCH_2CH(O)CH{=}CH_2 + NO_2$	1.4×10^{-11}	*b*	peroxy radicals reacting with NO to form alkoxy radicals along with nitrates
k_8	β-$HOCH_2CH(O_2)CH{=}CH_2 + NO \rightarrow$	β-$HOCH_2CH(ONO_2)CH{=}CH_2$	1.0×10^{-12}	7	
k_9	*Z*-$HOCH_2CH{=}CHCH_2O_2 + NO \rightarrow$	*Z*-$HOCHCH{=}CHCH_2OH + NO_2$	1.4×10^{-11}	*b*, *c*	
k_{10}	*Z*-$HOCH_2CH{=}CHCH_2O_2 + NO \rightarrow$	*Z*-$HOCH_2CH{=}CHCH_2ONO_2$	1.0×10^{-12}	7	
k_{11}	*E*-$HOCH_2CH{=}CHCH_2O_2 + NO \rightarrow$	*E*-$HOCH_2CH{=}CHCH_2O + NO_2$	1.4×10^{-11}	*b*	
k_{12}	*E*-$HOCH_2CH{=}CHCH_2O_2 + NO \rightarrow$	*E*-$HOCH_2CH{=}CHCH_2ONO_2$	1.0×10^{-12}	7	
k_{13}	β-$HOCH_2CH(O)CH{=}CH_2 \rightarrow$	$CH_2OH + CH_2CHCHO$	prompt	26	
k_{14}	*Z*-$HOCHCH{=}CHCH_2OH + O_2 \rightarrow$	$HO_2 + OCHCH{=}CHCH_2OH$	1.0×10^{-11}	26	chemistry of *Z*-δ-channel
k_{15}	*Z*-$HOCHCH{=}CHCH_2OH + NO \rightarrow$	*Z*-$HOCH(NO)CH{=}CHCH_2OH$	3.0×10^{-11}	26, 29–31	
k_{16}	*E*-$HOCH_2CH{=}CHCH_2O + O_2 \rightarrow$	*E*-$HOCH_2CH{=}CHCHO + HO_2$	1.0×10^{-11}	26	chemistry of *E*-δ-channel
k_{17}	*E*-$HOCH_2CH{=}CHCH_2O + NO \rightarrow$	*E*-$HOCH_2CH{=}CHCH_2ONO$	3.0×10^{-11}	26, 29–31	
k_{18}	$CH_2OH + O_2 \rightarrow$	$HCHO + HO_2$	9.8×10^{-12}	28	
k_{19}	$CH_2OH + NO \rightarrow$	CH_2OHNO	1.2×10^{-11}	27	
k_{20}	$OH + IHOC_4H_6 \rightarrow$	$IHOC_4H_6OH$	3.0×10^{-11}	*b*	
k_{21}	$HO_2 + NO \rightarrow$	$OH + NO_2$	1.2×10^{-11}	27	
k_{22}	$OH + NO \rightarrow$	HONO	9.4×10^{-13}	39	

[a] Rate constants are in molecule^{-1} cm^3 s^{-1} unless otherwise stated. [b] This work. [c] The formation of the *Z*-δ-hydroxy alkoxy radical and the subsequent isomerization to the *Z*-δ-di-hydroxy alkyl radical have been incorporated into one rate constant k_9 as the isomerization reaction is "prompt" on the experimental time scale.

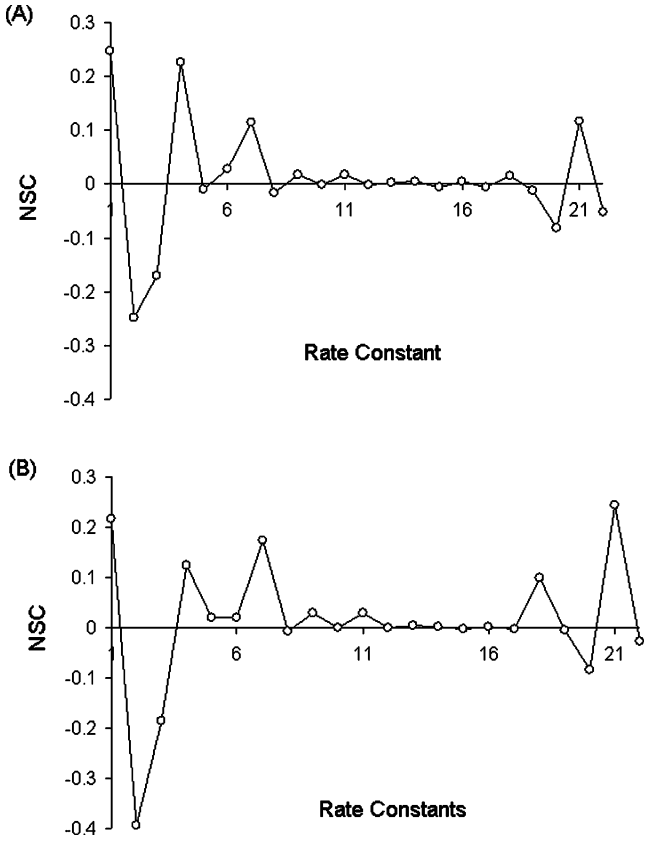

Figure 5. A. Sensitivity analysis at time 80 μs for $[IC_4H_6OH] = 3.0 \times 10^{13}$ molecules cm^{-3}, $[NO] = 1.9 \times 10^{15}$ molecules cm^{-3}, and $[O_2] = 6.5 \times 10^{16}$ molecules cm^{-3}, B. Sensitivity analysis at time 80 μs for $[IC_4H_6OH] = 3.0 \times 10^{13}$ molecules cm^{-3}, $[NO] = 9.6 \times 10^{14}$ molecules cm^{-3}, and $[O_2] = 6.5 \times 10^{16}$ molecules cm^{-3}.

for NO addition to the other hydroxy alkyl isomer generated by OH addition to the inner carbon of 1,3-butadiene[13] and agrees well with the rate constant of 1.2×10^{-11} cm^3 s^{-1} reported for NO addition to the hydroxy alkyl radical generated from OH addition to the outer carbon of isoprene.[21] The simulations are not sensitive to the rate constant for NO addition to CH_2OH, and we have adopted a slightly smaller value for this rate constant, that is, $k_{19} = 1.2 \times 10^{-11}$ cm^3 s^{-1}, which was reported previously.[27]

The O_2 addition to the hydroxyl alkyl radical plays an important role in atmospheric hydrocarbon oxidation as a chain propagation step leading to ozone formation. Although the very high ambient oxygen concentration in the troposphere renders accurate determination of this rate constant unnecessary for atmospheric modeling, an accurate value is needed for proper modeling of laboratory kinetic data. Given the sensitivity of the simulations to k_4 we can determine its value with moderate error limits. The rate constants k_3 and $(k_4 + k_5 + k_6)$ represent a set of parallel reactions leading toward chain termination and chain propagation, respectively. It is the competition between these two reactions, that is, k_3 [NO] and $(k_4 + k_5 + k_6)$ [O_2], that largely controls the shape of the OH profile. Thus, the value of k_3 affects determination of $(k_4 + k_5 + k_6)$, and the error in the determination of k_3 will be reflected in the error range of $(k_4 + k_5 + k_6)$. However, we rely on the numerous studies on the addition of NO to alkyl radicals which report rate constant values within a relatively narrow range.[13,21,27] A reasonable fit to our data can be obtained by using values ranging from 1.5×10^{-11} molecule^{-1} cm^3 s^{-1} to 3.0×10^{-11} molecule^{-1} cm^3 s^{-1} for the NO addition rate constant (k_3) (Figure S1, Supporting Information), and the best fit to the data is achieved for a value of 2.0×10^{-11} molecule^{-1} cm^3 s^{-1} for k_3. Using this value of 2.0×10^{-11} molecule^{-1} cm^3 s^{-1} for k_3, we find that the best fit to data is obtained by using the value of 7.0×10^{-13} molecule^{-1} cm^3 s^{-1} for the O_2 addition rate constant to the hydroxy radical $(k_4 + k_5 + k_6)$ with an upper limit of 1.3×10^{-12} molecule^{-1} cm^3 s^{-1} and a lower limit of 5.0×10^{-13} molecule^{-1} cm^3 s^{-1}. However, including the range of k_3 results in larger upper and lower limits for $(k_4 + k_5 + k_6)$ of 1.4×10^{-12} molecule^{-1} cm^3 s^{-1} and 4.0×10^{-13} molecule^{-1} cm^3 s^{-1}, respectively (Figure 6).

To our knowledge, there have been no detailed kinetics studies on the major addition channel of OH initiated butadiene oxidation. However, there have been extensive studies on isoprene oxidation, and given the similarity between isoprene

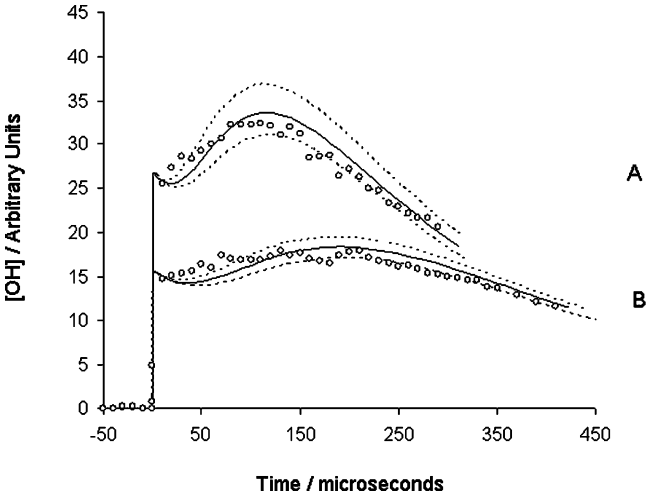

Figure 6. Dashed lines indicate the rate constants for estimated error range for O_2 addition to hydroxy alkyl radical. A. $[IC_4H_6OH] = 3.0 \times 10^{13}$ molecules cm^{-3}, $[NO] = 1.9 \times 10^{15}$ molecules cm^{-3}, and $[O_2] = 6.5 \times 10^{16}$ molecules cm^{-3}. Upper limit $= 1.4 \times 10^{-12}$ $molecule^{-1}$ cm^3 s^{-1}, lower limit $= 4.0 \times 10^{-13}$ $molecule^{-1}$ cm^3 s^{-1}. B. $[IC_4H_6OH] = 3.0 \times 10^{13}$ molecules cm^{-3}, $[NO] = 9.6 \times 10^{14}$ molecules cm^{-3}, $[O_2] = 6.5 \times 10^{16}$ molecules cm^{-3}. Upper limit $= 1.4 \times 10^{-12}$ $molecule^{-1}$ cm^3 s^{-1}, lower limit $= 4.0 \times 10^{-13}$ $molecule^{-1}$ cm^3 s^{-1}.

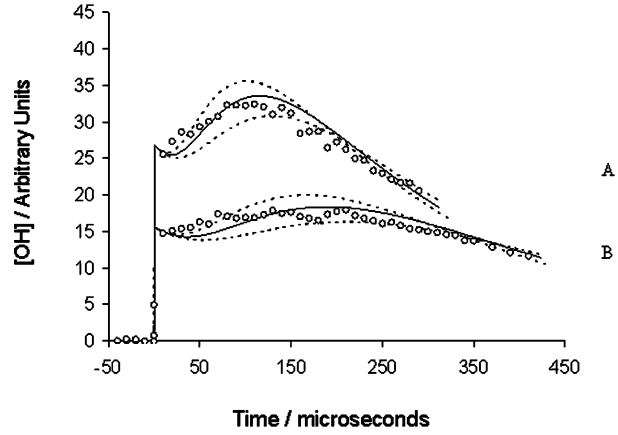

Figure 7. Dashed lines indicate the rate constants for estimated error range for NO reaction with hydroxy alkyl peroxy radical rate ($k_7 + k_8$). A. $[IC_4H_6OH] = 3.0 \times 10^{13}$ molecules cm^{-3}, $[NO] = 1.9 \times 10^{15}$ molecules cm^{-3}, and $[O_2] = 6.5 \times 10^{16}$ molecules cm^{-3}. Upper limit $= 2.5 \times 10^{-11}$$molecule^{-1}$ cm^3 s^{-1}, lower limit $= 9.0 \times 10^{-12}$ $molecule^{-1}$ cm^3 s^{-1}. B. $[IC_4H_6OH] = 3.0 \times 10^{13}$ molecules cm^{-3}, $[NO] = 9.6 \times 10^{14}$ molecules cm^{-3}, and $[O_2] = 6.5 \times 10^{16}$ molecules cm^{-3}. Upper limit $= 2.5 \times 10^{-11}$ $molecule^{-1}$ cm^3 s^{-1}, lower limit $= 9.0 \times 10^{-12}$ $molecule^{-1}$ cm^3 s^{-1}.

and butadiene, the mechanism of oxidation is expected to be similar. According to the theoretical study by Lei et al.,[32] the O_2 addition rate constant to the different hydroxy−isoprene isomers lies in the range of 1.0×10^{-13} cm^3 s^{-1} and 3.0×10^{-12} cm^3 s^{-1}, and our rate constant of $7^{+7.0}_{-3.0} \times 10^{-13}$ cm^3 s^{-1} lies within this range. Our rate constant is similar to the value of $(7.0 \pm 3.0) \times 10^{-13}$ cm^3 s^{-1} obtained from experimental studies by Zhang et al.[33] for the O_2 addition rate constant to hydroxy alkyl isoprene and within the mutual error limits of $(2.3 \pm 2.0) \times 10^{-12}$ cm^3 s^{-1} derived from OH cycling experiments on isoprene.[27]

The reaction of NO with peroxy radical is a crucial reaction in butadiene oxidation as its rate constant is a key factor in determining the relative importance of the NO−peroxy reaction and the peroxy−peroxy self- and cross-reactions. Under moderate to high concentrations of NO, consistent with urban environments, the peroxy radical reacts with NO to produce an energized nitrite species, which decomposes to form an alkoxy radical and NO_2 with a small fraction forming stable nitrate species.[34] These nitrates are stable compounds and are removed from the atmosphere via dry and wet deposition as well as long-range transport,[35] thus causing removal of NOx from atmosphere. Organic nitrates can also undergo photolysis and reaction with OH radical, and unsaturated nitrates can further react with O_3 and NO_3. These processes also cause removal of NOx from atmosphere. However, under low NOx conditions, such as the Amazon rain forest, peroxy radicals primarily undergo reaction with HO_2[36] or participate in self/cross-reactions with other peroxy radicals.[12] The rate constant for the NO reaction with peroxy radical to produce NO_2 and alkoxy radical (k_7) has a moderate sensitivity under our experimental conditions, but we are insensitive to the channel producing nitrate (k_8). Thus, we selectively determine k_7 and have assumed a value of 7% for the nitrate yield based on previous studies.[8] For the overall reaction of NO with the peroxy radicals, we have determined a rate constant of $1.5^{+1.0}_{-0.6} \times 10^{-11}$ cm^3 s^{-1}. Figure 7 shows the best fit (solid line) to the data obtained by using the above-mentioned value for ($k_7 + k_8$), and the dashed lines represent upper and lower limits of 2.5×10^{-11} $molecule^{-1}$ cm^3 s^{-1} and 9.0×10^{-12} $molecule^{-1}$ cm^3 s^{-1}, respectively. To our knowledge, this rate constant has not been reported for butadiene, although several studies have measured this rate constant for analogous systems. Zhang and co-workers performed a theoretical study on NO addition to isoprene peroxy radical and found the overall rate constant varying from 3.0×10^{-12} cm^3 s^{-1} to 2.0×10^{-11} cm^3 s^{-1} depending on the specific isomer,[34] and our reported rate constant lies within this range. Our rate constant also agrees well with the value of $(1.4 \pm 0.2) \times 10^{-11}$ cm^3 s^{-1} obtained by Maricq et al.[37] for NO + $CH_3(CO)O_2$ reaction and is also close to the value of 2×10^{-11} cm^3 s^{-1} recommended[38] by NASA-JPL for the same reaction. Our value is slightly higher than the range of $(9.0 \pm 3.0) \times 10^{-12}$ cm^3 s^{-1} obtained by Park et al.[27]

Reaction k_{13}, which corresponds to the decomposition of activated alkoxy radicals, is predicted to be fast compared to the time scale of the experiment.[27] This reaction is described as "prompt" in the reaction mechanism, and the experiment is insensitive to its absolute values for values higher than 1.0×10^6 s^{-1}. The reaction rate constants k_4, k_5, and k_6 in Table 3 correspond to relative branching ratios of different peroxy radicals. Reaction 4 corresponds to the branching to form β-hydroxy peroxy radicals, which subsequently react with NO to form β-hydroxy alkoxy radicals and decompose to form acrolein and formaldehyde molecules. Reaction 5 corresponds to the branching to form Z-δ-hydroxy peroxy radicals which undergo a prompt 1−5 hydrogen transfer reaction followed by hydrogen abstraction by oxygen to form 4-hydroxy-2-butenal and HO_2. Finally, reaction 6 describes the branching of the (E)-δ- hydroxy alkoxy radical which reacts with oxygen by hydrogen abstraction to form 4-hydroxy-2-butenal and HO_2 as its end products.[4] As a result of the inherent symmetry of 1,3-butadiene, both the (E)- and the (Z)-forms of δ-hydroxy alkoxy radical lead to the same final product. Thus, although 4-hydroxy-2-butenal has been detected in end product studies,[4] the branching between the two channels has not been measured nor calculated. A branching of 0.74 for the β-hydroxy alkoxy channel provides a good fit to the data and is based on the results of isotopic studies described in the following section. As in case of isoprene, the E- and Z-forms of the δ-hydroxy alkoxy radical are expected to have equivalent branching due to the very low barrier of E/Z interconversion,[14] and therefore we have assumed

TABLE 3: Summary of End Product Distributions (in percentage yield) Predicted by the Branching Ratios Determined in This Study, Assuming Initial Branching Ratios of 0.87:0.13 for Hydroxy Alkyl Radicals I and II (Figure 1)[a]

end product	current study	Berndt[4]	Baker[39]	Tuazon[8]	Sprengnether[22]
organic nitrate	7[a]	6 ± 2		7 ± 3	11 ± 6
acrolein	63 ± 10	59 ± 6	58 ± 10	58 ± 4	69 ± 7
4-hydroxy-2-butenal	21 ± 9	23 ± 10	25^{+15}_{-10}		
3-butenal (C_4 carbonyl)	9				
HCHO	63 ± 10	64 ± 8		62 ± 5	69 ± 10
furan		4.6 ± 1.4		3−4	1.9 ± 0.2

[a] The current study was insensitive to the nitrate yield and the value of 7% recommended by Tuazon et al. was adopted.[8] [a] Included for comparison are the end product distributions reported in other studies.

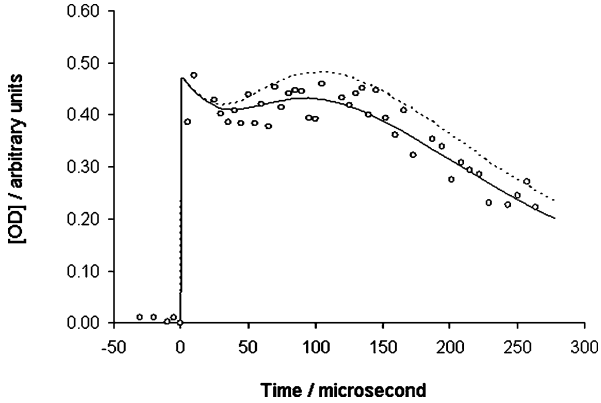

Figure 8. OD cycling from deuterated precursor. $[IC_4H_6OD] = 4.0 \times 10^{13}$ molecules cm^{-3}, $[NO] = 1.9 \times 10^{15}$ molecules cm^{-3}, and $[O_2] = 3.3 \times 10^{16}$ molecules cm^{-3}. The best fit was obtained for a branching of 13% for the *E*-*δ*-hydroxy peroxy channel.

that the same is true for 1,3-butadiene. However, our sensitivity analysis predicts that OH cycling experiments are not a sensitive test of the branching (reactions 5 and 6) necessitating isotopically labeled cycling experiments.

We note that the inclusion of a minor contribution (<4%) from the inner OH addition channel eliminates the short-term decay exhibited by the simulation but does not alter the long-term behavior.

B. OD Cycling from a Deuterated Precursor. As shown in Figure 4, if the OH group is replaced by an OD group, then the *β*-hydroxy peroxy radical and the (*Z*)- isomer of the *δ*-hydroxy peroxy radical both lead to the formation of OD while the (*E*)-isomer of the *δ*-hydroxy peroxy radical yields OH. Therefore, the detection of OD from a deuterated precursor should result in lower signals as compared to the previous OH cycling experiments using a nondeuterated precursor. It is this decrease in signal that corresponds to the yield of the (*E*)-*δ*-hydroxy peroxy channel. For this isotopic study, the precursor molecule was deuterated by dissolving it into D_2O and shaking for ∼30 min followed by extraction and purification of the organic compound. The LIF cell and the inlet lines were passivated by flowing D_2O for several hours to reduce H/D exchange by the hydrogen at surfaces.

Figure 8 shows the OD signal obtained following the photolysis of the deuterated precursor. The prompt rise due to the spontaneous dissociation of the nascent hydroxyalkyl radical to form OD and 1,3-butadiene is followed by a slight rise and decay. The data is very similar to the data from nonisotopic studies (Figure 3), yet with a smaller cycling signal relative to the prompt rise due to the absence of contribution of OD signal from the (*E*)-*δ*-hydroxy peroxy channel. This decrease in the cycling signal over prompt rise provides a quantitative measure of the branching of the (*E*)-*δ*-hydroxy peroxy channel. The dashed line is the simulation assuming no (*E*)-*δ*-hydroxy peroxy channel formation, whereas the solid line represents the best fit to this data corresponding to a branching of 13% for the (*E*)-*δ*-hydroxy peroxy channel. This measurement provides an upper limit to the branching of the (*E*)-*δ*-peroxy channel since there may be alternative chemistry not included in the model that is capable of producing OH from a deuterated precursor. The predicted equal branching for the *E*- and *Z*-isomers[14] results in an overall branching for the *δ*-hydroxy peroxy channel of 26%. This value matches very well with the overall branching of 25% for the *δ*-hydroxy peroxy channel reported by Jenkin and co-workers.[12] An error analysis of these simulation fits to data provides an estimated error range of ±5% for the branching of the *E*-channel, which provides an overall branching of 26 ± 10% for the *δ*-hydroxy peroxy channel.

Although the observation of OH from a deuterated precursor in the analogous isoprene system provided direct evidence of the *E*-channel, the low S/N in the current system precluded OH detection.

IV. Predicted First Generation End Product Distribution

On the basis of the 26 ± 10% branching to the *δ*-hydroxy peroxy channel and assuming an initial branching of 0.87:0.13 for isomers I and II (Figure 1)[12] and a nitrate yield of 7%, we predict a yield of 21 ± 9% for 4-hydroxy-2-butenal in close agreement to the value of 23 ± 10% reported by Berndt and Boge in a product study of the 1,3-butadiene−OH oxidation.[4] Our value is also very close to the product yield of (25^{+15}_{-10})% obtained by Baker and co-workers in their end product study.[39] Combining the current results for the dominant channel (Channel I in Figure 1) with our previous results for the minor channel of OH−1,3-butadiene oxidation chemistry, we can predict the end product distribution assuming a nitrate yield of 7%. The results are given in Table 3.

The yields of nitrate, acrolein, 4-hydroxy-2-butenal, and formaldehyde are predicted to be 7%, 63 ± 10%, 21 ± 9%, and 63 ± 10%, respectively. These predicted yields are very close to those found in other studies and lie within the mutual error limits. It is worth noting that since acrolein and HCHO are co-products from the same reaction they should be formed in equal yield as predicted by our model. Berndt and Boge[4] and Tuazon and co-workers[8] have reported slightly higher yield for HCHO compared to acrolein. Although the acrolein and HCHO yields are within their mutual error limits, the authors noted that there may be additional pathways leading to the formation of HCHO.[4,8] Our predicted yield for acrolein is slightly higher than values reported by Berndt and Boge[4] and Tuazon et al.[8] but is very close to their HCHO yields. The wall-less studies conducted by Sprengnether et al.[22] also reported equal yields for HCHO and acrolein, in good agreement with our values. On this basis, we suggest that there may be no additional pathways to the formation of HCHO. Berndt and Boge[4] and Tuazon and co-workers[8] also reported a furan yield

of 3−4%, resulting from a fraction of the *Z*-δ-hydroxy alkoxy channel via cyclization. Wall-less experiments on the OH initiated oxidation of isoprene did not detect the 3-methyl furan derivative,[22] suggesting that furan derivatives result from heterogeneous secondary reactions. However, the same group reported a low yield (1.9%) for furan from 1,3-butadiene oxidation, suggesting that a small fraction of *Z*-δ-hydroxy alkoxy channel may lead to furan. The current study only measures the branching ratio of the *E*-δ-hydroxy alkoxy channel and is insensitive to a small fraction of *Z*-δ-hydroxy alkoxy channel leading to furan. If some or all of the furan is formed through heterogeneous reaction, then the real yield of 4-hydroxy-2-butenal is likely to be slightly higher but will still be in the range of our reported yield. Thus our results are not inconsistent with a small yield of furan, but making any conclusion on furan ring formation is beyond the scope of this study. The C_4 carbonyl 3-butenal to our knowledge has not been reported. However, the analogous C_5 carbonyl compound arising from similar chemistry from isoprene has been detected previously.[20] Berndt and Boge[4] carried out the most comprehensive end product analysis but did not observe 3-butenal. However, their product yields account for 94% of reacted carbon including 4.6% of furan yield. Considering the combined uncertainties of product yields, and the fact that furan yield is most likely to be less than 4.6%, the formation of 3-butenal cannot be ruled out by the studies of Berndt and Boge.[4] The theoretical study of Park et al. has predicted the formation of the 3-butenal from the minor channel of OH-1,3-butadiene oxidation,[13] and we have used the reported branching ratios from that work.

V. Conclusions

We have reported the first isomeric selective study on the dominant channel of OH radical initiated oxidation of 1,3-butadiene. Laser photolysis of the monodeuterated/nondeuterated iodohydrin precursor molecule leads to the formation of a single isomer, the major addition adduct of OH-1,3-butadiene reaction, and OH/OD cycling experiments in the presence of NO and O_2 provides valuable information about the oxidation mechanism. We have employed sensitivity analysis to confirm that the experimental conditions were suitable for the determination of the isomeric selective rate constants. We have determined the rate constant of O_2 addition to the hydroxy alkyl radical to be $7^{+7.0}_{-3.0} \times 10^{-13}$ cm^3 s^{-1}, and we find a value of $1.5^{+1.0}_{-0.6} \times 10^{-11}$ cm^3 s^{-1} for the overall reaction rate constant of the hydroxy peroxy radical with NO. Isotopic cycling experiments permit quantification of the branching for the *E*-δ-hydroxy peroxy channel, and we find an upper limit for the branching to be 13 ± 5%. This isomeric selective kinetic study, together with a previous study[13] on the minor channel of the 1,3-butadiene oxidation, presents a clear overall picture of butadiene oxidation under high NOx condition relevant to most parts of the continental U.S.A.

Acknowledgment. The authors acknowledge the assistance of Dr. Jiho Park. This work was supported by the Environmental Protection Agency (EPA) and Texas Commission on Environmental Quality (TCEQ).

Supporting Information Available: ^{1}H NMR and ^{13}C NMR spectra and additional information. This material is available free of charge via the Internet at http://pubs.acs.org.

References and Notes

(1) United States Environmental Protection Agency. *Locating and Estimating Air Emissions from Sources of 1,3-Butadiene*; EPA-454/R-96-008; Office of Air Quality Planning and Standards: Research Triangle Park, NC, 1996.
(2) Vimal, D.; Pacheco, A. B.; Iyengar, S. S.; Stevens, P. S. *J. Phys. Chem. A* **2008**, *112*, 7227.
(3) Duffy, B. L.; Nelson, P. F. *Atmos. Environ.* **1997**, *31*, 3877.
(4) Berndt, T.; Boge, O. *J. Phys. Chem. A* **2007**, *111*, 12099.
(5) United States Environmental Protection Agency. *Health Assessment of 1,3-Butadiene*; EPA/600/P-98/001F; Office of Research and Development: Washington, DC, 2002.
(6) Cote, I. L.; Bayard, S. P. *Environ. Health Perspect.* **1990**, *86*, 149.
(7) Kligerman, A. D.; Doerr, C. L.; Milholland, V. S.; Tennant, A. H. *Toxicology* **1996**, *113*, 336.
(8) Tuazon, E. C.; Alvarado, A.; Aschmann, S. M.; Atkinson, R.; Arey, J. *Environ. Sci. Technol.* **1999**, *33*, 3586.
(9) Li, Z. J.; Nguyen, P.; de Leon, M. F.; Wang, J. H.; Han, K. L.; He, G. Z. *J. Phys. Chem. A* **2006**, *110*, 2698.
(10) Liu, X. Y.; Jeffries, H. E.; Sexton, K. G. *Atmos. Environ.* **1999**, *33*, 3005.
(11) Notario, A.; Le Bras, G.; Mellouki, A. *Chem. Phys. Lett.* **1997**, *281*, 421.
(12) Jenkin, M. E.; Boyd, A. A.; Lesclaux, R. *J. Atmos. Chem.* **1998**, *29*, 267.
(13) Greenwald, E. E.; Park, J.; Anderson, K. C.; Kim, H.; Reich, B. J. E.; Miller, S. A.; Zhang, R. Y.; North, S. W. *J. Phys. Chem. A* **2005**, *109*, 7915.
(14) Dibble, T. S. *J. Phys. Chem. A* **1999**, *103*, 8559.
(15) Lei, W. F.; Zhang, R. Y. *J. Phys. Chem. A* **2001**, *105*, 3808.
(16) Park, J.; Stephens, J. C.; Zhang, R. Y.; North, S. W. *J. Phys. Chem. A* **2003**, *107*, 6408.
(17) Dibble, T. S. *J. Phys. Chem. A* **2002**, *106*, 6643.
(18) Fan, J. W.; Zhang, R. Y. *Environ. Chem.* **2004**, *1*, 140.
(19) Zhao, J.; Zhang, R. Y.; North, S. W. *Chem. Phys. Lett.* **2003**, *369*, 204.
(20) Greenwald, E. E.; Ghosh, B.; Anderson, K. C.; Dooley, K. S.; Zou, P.; Selby, T.; Osborn, D. L.; Meloni, G.; Taatjes, C. A.; Goulay, F.; North, S. W. *J. Phys. Chem. A* **2010**, *114*, 904.
(21) Ghosh, B.; Bugarin, A.; Connell, B. T.; North, S. W. *J. Phys. Chem. A* **2010**, *114*, 2553.
(22) Sprengnether, M.; Demerjian, K. L.; Donahue, N. M.; Anderson, J. G. *J. Geophys. Res., [Atmos.]* **2002**, *107*, 13.
(23) McGivern, W. S.; Suh, I.; Clinkenbeard, A. D.; Zhang, R. Y.; North, S. W. *J. Phys. Chem. A* **2000**, *104*, 6609.
(24) Reitz, J. E.; McGivern, W. S.; Church, M. C.; Wilson, M. D.; North, S. W. *Int. J. Chem. Kinet.* **2002**, *34*, 255.
(25) Ianni, J. C. A Comparison of the Bader-Deuflhard and the Cash-Karp Runge-Kutta Integrators for the GRI-MECH 3.0 Model Based on the Chemical Kinetics Code Kintecus. In *Computational Fluid and Solid Mechanics*; Bathe, K. J., Ed.; Elsevier Science Ltd.: Oxford, U.K., 2003; pp 1368–1372.
(26) Atkinson, R.; Baulch, D. L.; Cox, R. A.; Hampson, R. F.; Kerr, J. A.; Troe, J. *J. Phys. Chem. Ref. Data* **1989**, *18*, 881.
(27) Park, J.; Jongsma, C. G.; Zhang, R. Y.; North, S. W. *J. Phys. Chem. A* **2004**, *108*, 10688.
(28) Glaschick Schimpf, I.; Leiss, A.; Monkhouse, P. B.; Schurath, U.; Becker, K. H.; Fink, E. H. *Chem. Phys. Lett.* **1979**, *67*, 318.
(29) Atkinson, R. *J. Phys. Chem. Ref. Data* **1997**, *26*, 215.
(30) Deng, W.; Wang, C. J.; Katz, D. R.; Gawinski, G. R.; Davis, A. J.; Dibble, T. S. *Chem. Phys. Lett.* **2000**, *330*, 541.
(31) Blitz, M.; Pilling, M. J.; Robertson, S. H.; Seakins, P. W. *Phys. Chem. Chem. Phys.* **1999**, *1*, 73.
(32) Lei, W. F.; Zhang, R. Y.; McGivern, W. S.; Derecskei-Kovacs, A.; North, S. W. *J. Phys. Chem. A* **2001**, *105*, 471.
(33) Zhang, D.; Zhang, R. Y.; Church, C.; North, S. W. *Chem. Phys. Lett.* **2001**, *343*, 49.
(34) Zhang, D.; Zhang, R. Y.; Park, J.; North, S. W. *J. Am. Chem. Soc.* **2002**, *124*, 9600.
(35) Chen, X. H.; Hulbert, D.; Shepson, P. B. *J. Geophys. Res., [Atmos.]* **1998**, *103*, 25563.
(36) King, M. D.; Thompson, K. C. *Atmos. Environ.* **2003**, *37*, 4517.
(37) Maricq, M. M.; Szente, J. J. *J. Phys. Chem.* **1996**, *100*, 12374.
(38) Sander, S. P.; Friedl, R. R.; Golden, D. M.; Kurylo, M. J.; Moortgat, G. K.; Wine, P. H.; Ravishankara, A. R.; Kolb, C. E.; Molina, M. J.; Finlayson-Pitts, B. J.; Huie, R. E.; Orkin, V. L. *Chemical Kinetics and Photochemical Data for Use in Stratospheric Modeling*; JPL Publ. 06-2; Jet Propulsion Lab: Pasadena, CA, 2006.
(39) Baker, J.; Arey, J.; Atkinson, R. *Environ. Sci. Technol.* **2005**, *39*, 4091.

JP1006878